DOI:10.7598/cst2017.1413
ISSN:2278-3458

Chemical Science Transactions
2017, **6(4),** 513-522

RESEARCH ARTICLE

Synthesis and Characterization of Various Metal Ions Doped CeO_2 Nanoparticles Derived from the *Azadirachta Indica* Leaf Extracts

S. PARVATHY[1*] and B. R.VENKATRAMAN[2]

[1]Department of Chemistry, Government Arts College (Autonomous),
Salem-636 007, Tamilnadu, India

[2]P.G. and Research Department of Chemistry, Periyar E.V.R.College (Autonomous),
Tiruchirappalli-620 023, Tamilnadu, India

chemparuvenkat@gmail.com

Received 10 May 2017 / Accepted 28 June 2017

Abstract: The cerium oxide nanoparticles (CeO_2 NPs) and M^{2+} doped CeO_2 NPs (M^{2+} = Zn^{2+}, Ni^{2+}, Cu^{2+} and Co^{2+}) were prepared through the *Azadirachta indica (A. indica*) leaf extracts. The x-ray diffraction studies confirmed that synthesized pure and M^{2+} doped CeO_2 NPs were exhibited the cubic structure. The FESEM and TEM images of both pure and M^{2+} doped CeO_2 NPs have exhibited spherical structure. From the EDAX spectral analysis, the elemental compositions were identified. The various functional groups were confirmed by FT-IR spectrum. Photoluminescence spectral analysis, small shift observed for emission of the CeO_2 NPs values as compared to that of the transition metal ions doped CeO_2 NPs emission values. The antimicrobial studies were performed against a set of gram positive (*Staphylococcus aureus* and *Streptococcus pneumoniae*) and gram negative (*Escherichia coli*, *Pseudomonas aeruginosa*, *Proteus vulgaris*, *Klebsiella pneumonia* and *Shigelladysenteriae*) bacterial and fungal *candida albicans* strain.

Keywords: CeO_2, Antimicrobial activity, FTIR, Photoluminscenance, FESEM, TEM

Introduction

Cerium oxide NPs are highly used rare earth compounds possessing wide applications in industrial and commercial products, which have been used for a variety of applications including sensors[1], membrane systems[2], fuel cells[3], mechanical polishing[4], ultraviolet absorbance[5], catalysis[2], medicine[6,7] and environmental chemistry[8].

Rare earth oxides nanoparticles are used in biomedical applications like radical scavenging of antioxidants[14,15]. The biomedical properties of metal oxide nanoparticles have been studied in recent years. Among the rare-earth oxides CeO_2 NPs are widely used for biological applications have mostly involved the consumption of mammalian cells[9-11]. However, the CeO_2 NPs are effectively used in cancer treatment[12] and inflammation[13]

through controlling the reactive oxygen species levels. As the size of the material becomes smaller and the band gap becomes larger, this changes the optical and electrical properties of the material, making it suitable for new applications and devices. Among them, the widely accepted method to modify the electrical and optical properties of a semiconductor is the addition of impurity atoms, or doping[16,17].

The antimicrobial activity of CeO_2 NPs can also be explained as follows. ROS include the most reactive hydroxyl radical ($^{\bullet}OH$), less toxic superoxideanion radical ($^{-\bullet}O_2$) and singlet oxygen ($^1O_2$) with a weaker oxidizer, contributing to the major oxidative stress in biological systems[18]. ROS generation is closely associated with the efficiency of a photocatalyst, depending on the generation rate, rate of migration and energy levels of the photoexcited electron-hole pairs. The enhancement of ROS yields may be connected with the electronic properties and microstructure (*i.e*., grain size, specific surface area and pore, *etc*.) of the nanostructure[19] of the CeO_2 NPs.

In the present work, pure and transition metal ion (Zn^{2+}, Ni^{2+}, Cu^{2+} and Co^{2+})-doped CeO_2 NPs are prepared through the *Azadirachta indica* leaf extract. The synthesized nanoparticles are characterization done by the structural, morphological, optical and antimicrobial properties of pure and transition metal ion (Zn^{2+}, Ni^{2+}, Cu^{2+} and Co^{2+})-doped CeO_2 NPs.

Experimental

The following high purity chemicals such as cerium nitrate, zinc nitrate, nickel nitrate, copper nitrate and cobalt nitrate were used as precursors without further purification. The 10 g of *Azadirachta indica* finely cut leaves were added to 100 mL of double distilled water and boiled at 50-60 °C for 10 min. The obtained extraction was filtered using Whatmann No. 1 filter paper and the filtrate were collected in 250 mL Erlenmeyer flask and stored at room temperature for further usage. Thereafter, 0.1 M of $CeNO_3$ salt was added to 100 mL of *A. indica* leaf extract. This solution was stirred constantly at 80 °C temperature for 6 h. A brown precipitate formed and then it was become a yellowish brown in color on continuous stirring. Finally, the precipitate was dried at 120 ^oC.

Similarly, for the preparation of transition metal-doped CeO_2 NPs, in the case of Zn-doped samples, 0.095 M of aqueous cerium nitrate salt and 0.005 M zinc nitrate salt were added to 100 mL of *Azadirachta indica* leaf extract; a brown precipitate formed and then it was become a yellowish brown in color on continuous stirring. This solution was stirred constantly at a temperature of 80 ^oC for 6 h. Finally, the precipitate was dried at 120 ^oC, we get the Zn doped CeO_2 sample. The same procedure followed for the preparation of the Ni, Cu and Co-doped CeO_2 samples for which nickel nitrate, copper nitrate and cobalt nitrate were used respectively. Thus, pure and transition metal ions-doped CeO_2 NPs samples were obtained. Further the precipitates were annealed at 400 °C for 5 h. Thus, CeO_2 NPs were obtained.

Antibacterial assay

The antibacterial activity of the CeO_2 and transition metal ion (Zn^{2+}, Ni^{2+}, Cu^{2+} and Co^{2+})-doped CeO_2 NPs were carried out by the well diffusion method against the bacterial strains of *K. pneumonia, S. aureus, S. dysenteriae, E. coli, P. aeruginosa, S. pneumonia and P. vulgaris* on Mueller hinton agar, according to the clinical and laboratory standards institute (CLSI)[20]. The media plate's Mueller hinton agar (MHA) was streaked with bacteria 2-3 times by rotating the plate at 60˚ angles for each streak to ensure the homogeneous distribution of the inoculums. After inoculation, discs (6 mm Hi-Media) 2 mg, of the test samples were placed on the bacteria-seeded well plates using micropipettes.

The plates were then incubated at 37 ^{o}C for 24 h. The inhibition zone around the well was measured and recorded. Amoxicillin (Hi-Media) was used as the positive controls against gram +ve and gram –ve bacteria respectively. The positive controls results were as compared to that of the efficacy of the test CeO_2, Zn:CeO_2, Cu:CeO_2, Ni:CeO_2 and Co:CeO_2, NPs samples.

Antifungal assay

Antifungal activity was determined by an agar well diffusion method against the test fungi *Candida albicans* using potato dextrose agar. The test strain was transferred into potato dextrose broth (PDB) and incubated at 37 °C until it achieved the turbidity of 0.5 McFarland standards. The media plates were inoculated with the test strain by streaking for 2-3 times by rotating the plate at a 60° angle for each streak to ensure uniform distribution of noculums. Subsequently, sterile disc (6 mm) loaded with 2 mg of test samples (CeO_2 and transition metal ion doped CeO_2 NPs) were placed onto the inoculated well plates using micropipettes and incubated at 37 °C for 24 h under visible light. The zone of inhibition formed around the well was measured and recorded.

Characterization techniques

The pure CeO_2 and transition metal ion (Zn^{2+}, Ni^{2+}, Cu^{2+} and Co^{2+})-doped CeO_2 NPs were characterized by x-ray diffractometer (model: X'PERT PRO PAN alytical). The diffraction patterns were recorded in the range of 20^{o}-80^{o} for the CeO_2 NPs samples, where the monochromatic wavelength of 1.54 Å was used. The samples were analyzed by field emission scanning electron microscopy (Carl Zeiss Ultra 55 FESEM) with EDAX (model: Inca). TEM analyses were carried out by the instrument Philips CM 200 model operated at an accelerating voltage of 20-200kv Resolution: 2.4 A. The FT-IR spectra were recorded in the range of 400-4000 cm^{-1} by using a Perkin-Elmer spectrometer. Photoluminescence spectra were measured using Cary Eclipse spectrometer.

Results and Discussion

X-ray diffraction studies

The XRD patterns of pure and transition metal ion (Zn^{2+}, Ni^{2+}, Cu^{2+} and Co^{2+})-doped CeO_2 NPs are shown in Figure 1. The diffraction pattern corresponds to the cubic phase of CeO_2. The XRD peaks are located at angles (2θ) of 28.53, 33.00, 47.51, 56.61 and 76.34 corresponding to (111), (200), (220), (311), (222) and (331) planes of the CeO_2 NPs respectively. The face-center cubic phase of CeO_2 NPs exactly matches JCPDS data card no: 34-0394. Also observed that, there is no impurity phases found to (Zn^{2+}, Ni^{2+}, Cu^{2+} and Co^{2+})-doped CeO_2 samples because of the substitution in smaller ionic radii Zn (0.74 Å), Ni (0.69 Å), Cu (0.73 Å) and Co (0.745 Å). Furthermore, the 2θ values have small shifted occur, because of successfully doped the transition metal ion (Zn^{2+}, Ni^{2+}, Cu^{2+} and Co^{2+}) in the CeO_2 crystal structure demonstrating the formation of homogeneous Ce-Zn-O, Ce-Ni-O, Ce-Cu-O and Ce-Co-O solid solution. The lattice constant 'a' of CeO_2 can be calculated by using the relation,

$$\frac{1}{d^2} = \left(\frac{h^2 + k^2 + l^2}{a^2} \right) \quad (1)$$

The lattice constant 'a' is obtained through the relation $a = \sqrt{d^2(h^2+k^2+l^2)}$. The calculated 'a' values are 5.4108 Å, 5.3710 Å, 5.4685 Å, 5.4190 Å and 5.4687 Å for pure and (Zn, Ni, Cu and Co)-doped CeO_2 NPs respectively. The diffraction peaks of (Zn, Ni, Cu and Co)-doped

CeO_2NPs are small shifted to diffraction angles relative to those of the pure CeO_2 NPs, indicating the variation in lattice constant upon doping with Zn, Ni, Cu and Co ions. It is suggests that (Zn, Ni, Cu and Co) ions are incorporated into the CeO_2 matrix.

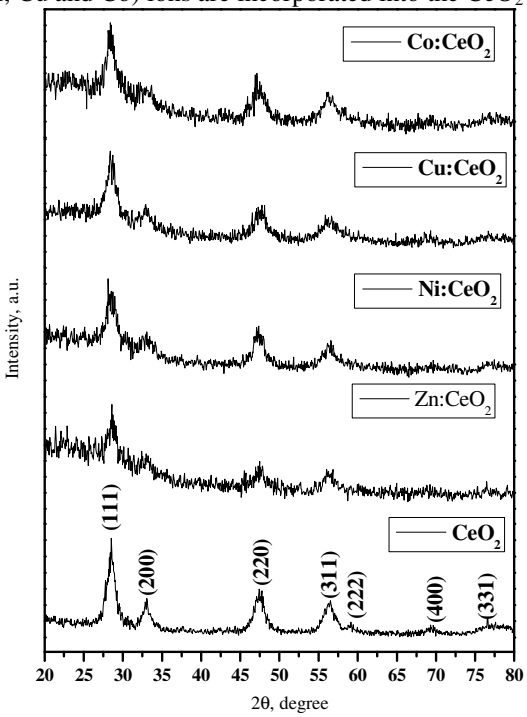

Figure 1. X-ray powder diffraction pattern of the pure and transition metal ion (Zn^{2+}, Ni^{2+}, Cu^{2+} and Co^{2+})-doped CeO_2 NPs

The average crystallite size D of the sample is calculated after appropriate background corrections from x-ray line broadening of the diffraction peaks using Debye-Scherrer's formula.

$$\text{Average crystallite size } D = \frac{0.9\lambda}{\beta \cos\theta}$$

Where λ is the wavelength of x-ray used (1.5405 A), β is the angular peak width at half maximum in radians and θ is the Bragg's diffraction angle. The average crystallite sizes are found to be 9.2 nm, 8.3 nm, 10 nm, 6.9 nm and 16.6 nm for pure and transition metal ion (Zn, Ni, Cu and Co)-doped CeO_2 NPs respectively. The average crystallite size decreased in the (Zn^{2+} and Cu^{2+})-doped CeO_2 NPs and increased in the (Ni^{2+} and Co^{2+})-doped CeO_2 NPs respectively. These changes in the particle size are mainly due to the distortion in the host CeO_2 lattice by foreign impurities *i.e.*, Zn^{2+}, Ni^{2+}, Cu^{2+} and Co^{2+}. From the above result revealed that the Cu doped CeO_2 more photocatalytic effect as compared to that of the pure and other transition metal ions (Zn^{2+}, Ni^{2+} and Co^{2+})-doped CeO_2 NPs and also it might be exhibit better antimicrobial activity.

Morphology and Elemental compositions

The surface morphology and elemental composition of pure and transition metal ion (Zn^{2+}, Ni^{2+}, Cu^{2+} and Co^{2+})-doped NPs are shown in Figure 2. The FESEM (Field Emission Scanning Electron Microscope) and TEM image clearly shows the average sizes of the NPs are

in nanometer range. The pure and transition metal ion (Zn, Ni, Cu and Co)-doped CeO_2 NPs are exhibits spherical structure. The SAED pattern (Selected Area Electron Diffraction, Figure 2), the reflection peaks are (111), (200), (220), (311), (222), (400), (331) and (420) of face center cubic structure for CeO_2 NPs. There are no additional rings in the SAED pattern stemming from any crystalline impurities for of pure and transition metal ion (Zn^{2+}, Ni^{2+}, Cu^{2+} and Co^{2+})-doped CeO_2 NPs. The typical EDAX spectra of pure and doped CeO_2 NPs are shown in Figure 2. The concentrations of transition metal ions (Zn, Ni, Cu and Co) percentage were found to be 2.01%, 2.17%, 2.34 and 2.38 % respectively. In the pure CeO_2 NPs, the atomic percentage of Ce, C and O were found to be 64.03 %, 20.15% and 15.82% respectively. However, for the transition metal ion (Zn^{2+}, Ni^{2+}, Cu^{2+} and Co^{2+})-doped CeO_2 NPs, the cerium percentage increased and whereas the oxygen percentage also increased, this is due to the doping effects.

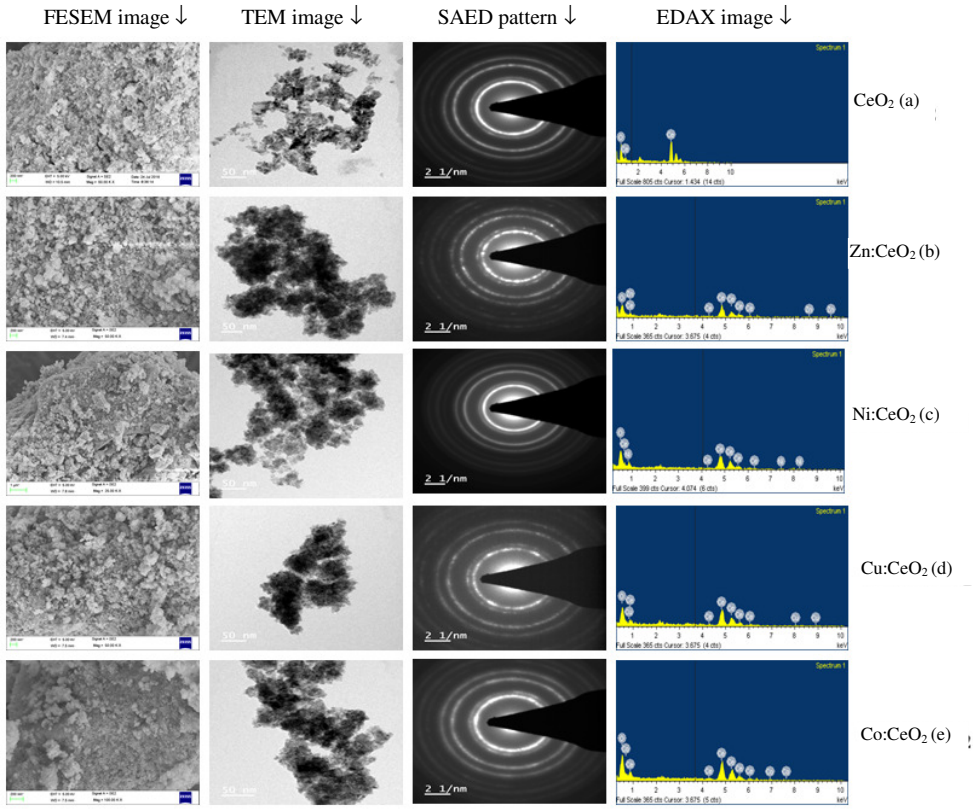

Figure 2. FESEM, TEM and EDAX analysis of (a) CeO_2 NPs (b) Zn:CeO_2, (c) Ni:CeO_2, (d) Cu:CeO_2 and (e) Co: CeO_2 NPs

FTIR analysis

Figure 3 shows the FTIR spectra of pure and transition metal ion (Zn^{2+}, Ni^{2+}, Cu^{2+} and Co^{2+})-doped CeO_2 NPs**.** In present work, the CeO_2 NPs characteristic vibration mode of Ce-O stretching vibration are observed at (982, 840, 702, 537 and 429 cm^{-1}), (982, 839, 702 and 427 cm^{-1}), (982, 840, 702, 531 and 409 cm^{-1}), (982, 840, 721, 522 and 429 cm^{-1}) and (984, 852, 700 and 542 cm^{-1}) for pure and transition metal ions doped CeO_2 NPs samples. The Ce-O-Ce stretching bands are found at (1114 and 1052 cm^{-1}), (1114 and 1053 cm^{-1}),

(1112 and 1054 cm^{-1}), (1113 and 1054 cm^{-1}) and (1113 and 1054 cm^{-1}) for pure and transition metal ion (Zn^{2+}, Ni^{2+}, Cu^{2+} and Co^{2+})-doped CeO_2 NPs respectively[21,2]. The H-O-H weak bending vibration band centered at 1630 cm^{-1}, 1697 cm^{-1}, 1626 cm^{-1} and 1628 cm^{-1} for pure and transition metal ion (Zn, Ni and Cu)-doped CeO_2 NPs samples. The O-H stretching vibration of water molecules range 3750-3000 $cm^{-1}$is assigned for Ce-OH[23,24]. From IR result, the broad absorption band found at 3389 cm^{-1}, 3371 cm^{-1}, 3374 cm^{-1}, 3404 cm^{-1} and 3393 cm^{-1} are attributed to the Ce-OH mode for pure and transition metal ion (Zn, Ni, Cu and Co)-doped CeO_2NPs respectively.

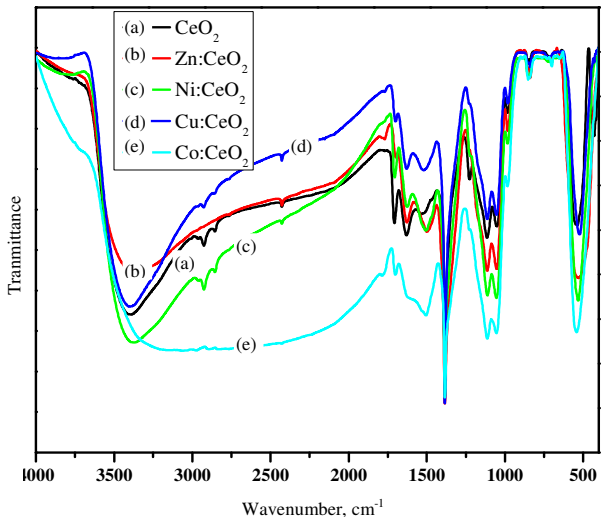

Figure 3. FT-IR spectra of the pure and transition metal ion (Zn^{2+}, Ni^{2+}, Cu^{2+} and Co^{2+})-doped CeO_2 NPs

Photoluminescence analysis

The photoluminescence (PL) spectra of the synthesized pure and transition metal ion (Zn^{2+}, Ni^{2+}, Cu^{2+} and Co^{2+})-doped CeO_2 NPs were recorded with the excited wavelength of 325 nm. The PL emission values are observed for pure and transition metal doped CeO_2 NPs, from the very short wavelength of 350 nm to the longer wavelength of 550 nm. A good fit with eight peaks using a Gaussian function was obtained. The PL spectra of the pure CeO_2 NPs emission are 361, 378, 391, 412, 444, 460, 490 and 522 nm values given in Table 1.

Table 1. Photoluminescence emission values of pure CeO_2 and transition metal ion doped CeO_2 NPs

CeO_2, nm	$Zn:CeO_2$, nm	$Ni:CeO_2$, nm	$Cu:CeO_2$, nm	$Co:CeO_2$, nm
361	361	361	361	360
378	377	379	377	376
391	390	392	390	388
412	410 and 411	412	411	411 and 412
444	444	444	423 and 438	444
460	-	-	-	-
490	490	490	490	490
522	521	522	524	521

The three near band edge emissions are observed at (361 nm, 378 nm and 391 nm) for CeO_2 NPs respectively, this NBE emission is attributed to a band-to-band recombination process, possibly involving localized or free exciton[24]. The violet emission band centered at 412 nm for CeO_2 NPs is attributed to defect states existing extensively between the Ce 4f state and O 2p valence band[25]. The two blue emissions are observed at 444 nm and 460 nm for CeO_2 NPs and this is due to localization of the energy levels between the Ce 4f band and the O 2p band. The blue-green emission located at 490 nm is possibly due to surface defects in the CeO_2 NPs respectively. The green emission peaks observed at 522 nm is due to the low density of oxygen vacancies.

In PL spectra, small shift observed for transition metal ion (Zn^{2+}, Ni^{2+}, Cu^{2+} and Co^{2+})-doped CeO_2 NPs emission values as compared to that of the CeO_2 NPs emission values. This is due to the defect state localized in between the Ce 4f and O 2p levels, lead to this small shift. These changes in the emissions confirmed the substitution of the transition metal ion (Zn^{2+}, Ni^{2+}, Cu^{2+} and Co^{2+}) into the CeO_2NPs lattice surface.

Antimicrobial studies

Pure and transition metal ions (Zn^{2+}, Ni^{2+}, Cu^{2+} and Co^{2+})-doped CeO_2 NPs tested against gram-positive bacteria (*S. aureus* and *S. neumonia*) and gram-negative bacteria (*E. coli*, *P. aeruginosa*, *P. vulgaris*, *K. pneumonia* and *S. dysenteriae*) and fungal species *candida albicans* studied well diffusion method are shown in Figure 4. Figure 5 and 6 shows the size of the zone of inhibition and antimicrobial activity formed around each well concentration 2 mg of pure and transition metal ions (Zn^{2+}, Ni^{2+}, Cu^{2+} and Co^{2+})-doped CeO_2 NPs loaded with test samples.

The inhibition zone of Cu doped CeO_2NPs possesses more antimicrobial activity than pure and other transition metal ion (Zn^{2+}, Ni^{2+} and Co^{2+})-doped CeO_2NPs. The antimicrobial activity of NPs may either directly interact with the microbial cells or to produce secondary products that cause damage. There are several mechanisms behind the antimicrobial activity of metal oxide nano materials. The antimicrobial mechanism, the CeO_2 NPs can be active by UV light, to increase electron-hole pairs.

- These holes split the H_2O molecule from the suspension of CeO_2 into hydroxyl radical ($OH^{\cdot}$) and hydrogen ion (H^+). Dissolved oxygen molecules are converted to superoxide radical anions ($^{\cdot}O_2^-$) which react with hydrogen ion (H^+) to produce $HO_2^{\cdot}$ radical.
- These hydroxyl radicals on collision with electrons produce hydrogen peroxide HO_2 anions, which is react with hydrogen to produce H_2O_2 molecules.
- The generated H_2O_2 molecules can penetrate the cell membrane and arrest the biological process in the bacteria.

The negatively charged particles of hydroxyl radicals OH^- and O_2^- super oxide radical anions cannot penetrate into the cell membrane and must remain in contact with the outer surface of the microbial[26,27]. But the active anionic molecules are effective toxic to microbial substance. In addition, the damage of cell membrane might directly lead to the leakage of minerals, proteins and genetic materials causing ultimate cell death[28,29]. The mechanism involved in the generation of reactive oxygen species from CeO_2 nanoparticles induced by UV light.

$$CeO_2 + h\upsilon \rightarrow CeO_2(e^-) + CeO_2(h^+) \quad (1)$$

$$CeO_2(h^+) + H_2O \rightarrow CeO_2 + {}^{\bullet}OH^- + H^+ \quad (2)$$

$$CeO_2(h^+) + OH^- \rightarrow CeO_2 + OH \quad (3)$$

$$CeO_2(e^-) + O_2 \rightarrow CeO_2 + {}^{\bullet}O_2^- \quad (4)$$

$$^{\bullet}O_2^- + H^+ \rightarrow HO_2^{\bullet} \text{ and}$$

$$2HO_2^{\bullet} \rightarrow O^2 + H_2O_2$$

The smaller sized NPs indeed have higher antibacterial activity[29]. From the XRD patterns, the particle size of pure and transition metal ions (Zn^{2+}, Ni^{2+}, Cu^{2+} and Co^{2+})-doped CeO_2 NPs are found at 9.2 nm, 8.3 nm, 10 nm, 6.9 nm and 16.6 nm respectively. The particle size of Cu doped CeO_2NPs are decreased as compared to that of the pure and other (Zn, Ni and Co) doped CeO_2 NPs, smaller size can easily penetrate into bacterial membranes due to their large interfacial area, thus enhancing their antimicrobial efficiency. During the generation of ROS, the unsaturated fatty acids in the cell membrane will be oxidized by $^{\bullet}OH$ group and affect the fluidity of cell membranes. Consequently decreased the thickness of bacteria cell wall and caused to bacteria death.

From the photoluminescence spectra, wavelengths of the green emissions values are at 522 nm, 521 nm, 522 nm, 524 nm and 521 nm for pure and (Zn^{2+}, Ni^{2+}, Cu^{2+} and Co^{2+})-doped CeO_2 NPs. This demonstrated the increased number of oxygen vacancies and interstitial oxygen vacancies in the Cu-doped CeO_2 NPs, leading to a higher number of ROS as compared to that of the pure and transition metal ion (Zn^{2+}, Ni^{2+} and Co^{2+})-doped CeO_2 NPs. The Cu-doped CeO_2 NPs possessed the potential to exhibit spontaneous ROS (reactive oxygen species) production based on material composition and surface characteristics.

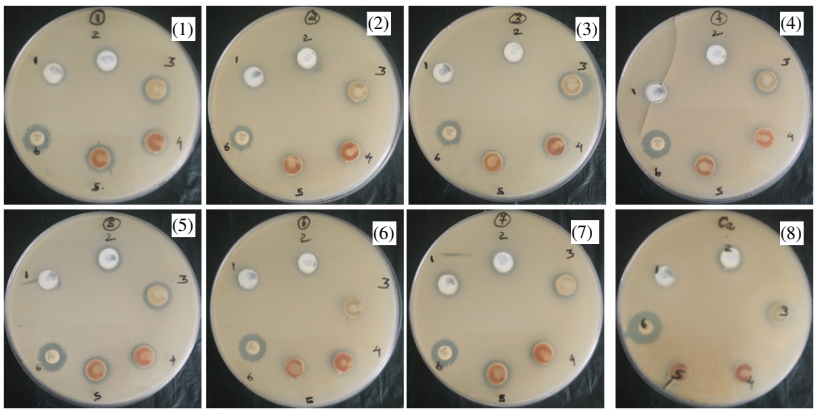

Figure 4. The antimicrobial activity of the Compounds against gram-positive *i.e* (1) *S. aureus* (2) *S. pneumonia* and gram-negative *i.e* (3) *E. coli* (4), *P. aeruginosa* (5), *P. vulgaris* (6), *K. pneumonia* and (7) *S. dysenteriae* and (8) *Candida albicans*

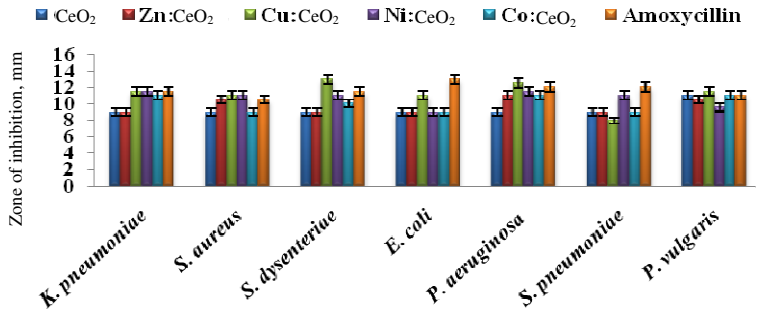

Figure 5. Antibacterial activity of CeO_2 and transition metal ion (Zn^{2+}, Ni^{2+}, Cu^{2+} and Co^{2+})-doped CeO_2 NPs against gram +ve and gram −ve bacterial strains

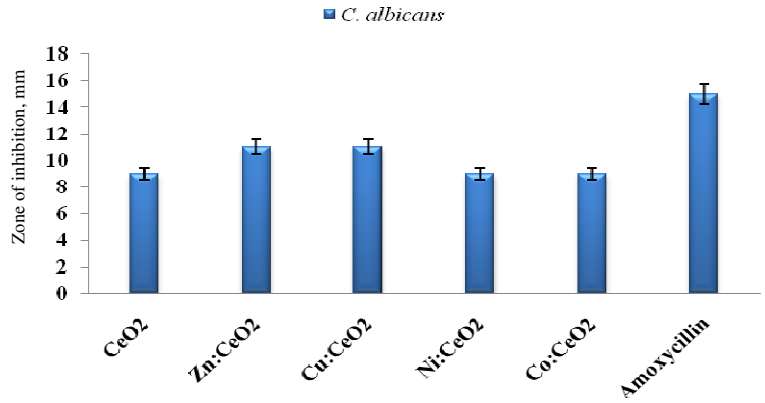

Figure 6. Anti-fungal activity of CeO_2 and transition metal ion (Zn^{2+}, Ni^{2+}, Cu^{2+} and Co^{2+})-doped CeO_2 NPs against *C. albicans* strains

Conclusion

Pure and transition metal ion (Zn^{2+}, Ni^{2+}, Cu^{2+} and Co^{2+})-doped CeO_2 NPs were prepared through the *Azadirachta indica* leaf extracts. From the x-ray diffraction studies the synthesized pure and transition metal ion (Zn^{2+}, Ni^{2+}, Cu^{2+} and Co^{2+})-doped CeO_2 NPs were exhibited cubic phase. The average particle sizes of M^{2+} doped CeO_2 low compare to pure CeO_2. From the FESEM and TEM images, the synthesized pure and transition metal ions-CeO_2 NPs were exhibited spherical structure. Elemental compositions were identified by EDAX spectra. From the FT-IR spectra, the various vibrational frequencies were assigned for the pure CeO_2 and transition metal ion-doped CeO_2 samples. From PL spectra, the transition metal ion (Zn^{2+}, Ni^{2+}, Cu^{2+} and Co^{2+})-doped CeO_2 NPs emission were small shift occurred as compared to that of pure CeO_2 NPs. These changes in the emissions were confirmed the substitution of the transition metal ions Zn^{2+}, Ni^{2+}, Cu^{2+} and Co^{2+} into the CeO_2 NPs lattice surfaces.

The antimicrobial studies performed against a set of bacterial and fungal strains showed that the Cu doped CeO_2 NPs possessed higher antimicrobial activity than the pure and other transition metal ion (Zn, Ni and Co)-doped CeO_2 NPs. So that, smaller size can easily penetrate into bacterial membranes due to their large interfacial area, thus enhancing their antimicrobial efficiency. The XRD data good agreement with these results.

References

1. Jasinski P, Toshio S and Harlan U A, *Sensors Actuators B: Chem.,* 2003, **95(1-3)**, 73-77; DOI:10.1016/S0925-4005(03)00407-6
2. Masui T, Tetsuya O, Ken-ichi M and Gin-ya A, *J Alloys Compounds,* 2000, **303,** 49-55; DOI:10.1016/S0925-8388(00)00603-4
3. Esposito V and Enrico T, *J Am Ceramic Soc.,* 2008, **91(4)**, 1037-1051; DOI:10.1111/j.1551-2916.2008.02347.x
4. Armini S, Joke D M, Whelan C M, Mansour M and Karen M, *J Electrochem Soc.,* 2008, **155(9)**, H653-H660; DOI:10.1149/1.2949085
5. Tsunekawa S, Sivamohan R, Ohsuna T, Takahashi H and Tohji K, *Mat Sci Forum*, 1999, **315**, 439-445; DOI:10.4028/www.scientific.net/MSF.315-317.439
6. Mandoli C, Francesca P, Stefania P, Giancarlo F, Paolo D N, Silvia L and Enrico T, *Adv Funct Mat.*, 2010, **20**, 1617-1624; DOI:10.1002/adfm.200902363

7. Colon J, Luis H, Joshua S, Swanand P, Chris K, Patrick K, Sudipta S, Wayne J D, and Cheryl H B, *Nanomed: Nanotechnol Biol Med.,* 2009, **5(2)**, 225-231; DOI:10.1016/j.nano.2008.10.003
8. Sun C, Hong L and Liquan C, *Energy Environmental Sci.,* 2012, **5**, 8475-8505; DOI:10.1039/C2EE22310D
9. Asati A, Santimukul S, Charalambos K, Sudip N and Manuel P, *AngewandteChemie International Edition*, 2009, **48(13)**, 2308-2312; DOI:10.1002/anie.200805279
10. Karakoti A S, Monteiro-Riviere N A, Aggarwal R, Davis, Roger J. Narayan, Self W T, McGinnis J and Seal S, *JOM J Minerals, Metals Materials Society,* 2008, **60(3)**, 33-37.
11. Lord M S, MoonSun J, Wey Yang T, Cindy G, James A,Vassie R A and John M W, *Biomaterials,* 2012, **33(31)**, 7915-7924; DO:10.1016/j.biomaterials.2012.07.024
12. Gao Y, Kan C, Jin-lu M and Fei G, *OncoTargets Therapy,* 2014, 7, 835-840; DOI:10.2147/OTT.S62057
13. Hirst S M, Ajay S K, Ron D T, Nammalwar S, Sudipta S and Christopher M R, *Small,* 2009, **5(24)**, 2848-2456; DOI:10.1002/smll.200901048
14. Kumar A, Suresh B, Ajay Singh K, Alfons S and Sudipta S, *Langmuir,* 2009, **25(18),** 10998-11007; DOI:10.1021/la901298q
15. Karakot A S, Monteiro-Riviere N A, Aggarwal R, Davis J P, Roger J N, Self W T, McGinnis J and Seal S, *JOM J Minerals, Metals Materials Society,* 2008, **60(3)**, 33-37.
16. Umaralikhan L and Jamal Mohamed Jaffar M, *J Mat Sci: Materials in Electronics,* 2017, **28(11),** 7677-7685; DOI:10.1007/s10854-017-6461-1
17. Hsu L, Yeh C S, Kuo C C, Huang B R and Dhar S, *J Optoelectronics Adv Mat.,* 2005, **7(6)**, 3039-3046.
18. Li Y, Wen Z, Junfeng N and Yongsheng C, *Acs Nano.,* 2012, **6(6)**, 5164-5173; DOI:10.1021/nn300934k
19. Arumugam A, Karthikeyan C, HajaHameed A S, Gopinath K, Gowri S and Karthika V, *Materials Science Engg: C,* 2015, **49**, 408-415; DOI:10.1016/j.msec.2015.01.042
20. Wright G D, *Chem Biology,* 2000, **7(6)**, R127-R132; DOI:10.1016/S1074-5521(00)00126-5
21. Yan B and Hongxia Z, *J Nanopart Res.,* 2008, **10(8)**, 1279; DOI:10.1007/s11051-008-9371-6
22. Mazaheri M, Tabrizi S A H, Aminzare M and Sadrnezhaad S K, Procedding of 11th ECERS Conference, Krakow, 2009, 655-658.
23. Choudhury B, Pawan C and Amarjyoti C, *J Experimental Nanosci.,* 2015, **10(2)**, 103-114; DOI:10.1080/17458080.2013.801566
24. Wang L, Jiawen R, Xiaohui L, Guanzhong L and Yanqin W, *Mat Chem Phys.,* 2011, **127(1-2)**, 114-119; DOI:10.1016/j.matchemphys.2011.01.043
25. Morshed A H, Moussa M E, Bedair S M, Leonard R, Liu S X and El-Masry N, *Appl Phys Lett.,* 1997, **70(13),** 1647; DOI:10.1063/1.118658
26. Tam K H, Djurišić A B, Chan C M N, Xi Y Y, Tse C W, Leung Y H, Chan W K, Leung F C C and Au D W T, *Thin Solid Films,* 2008, **516(18)**, 6167-6174; DOI:10.1016/j.tsf.2007.11.081
27. Karunakaran C, Rajeswari V and Gomathisankar P, *J Alloys Compd.,* 2010, **508(2)**, 587-591; DOI:10.1016/j.jallcom.2010.08.128
28. Zhang L, Yunhong J, Yulong D, Nikolaos D, Lars J, Malcolm P, Alex J O'N and David W Y, *J Nanoparticle Res.,* 2010, **12(5)**, 1625-1636; DOI:10.1007/s11051-009-9711-1
29. Zhang L, Yulong D, Malcolm P and David Y, *Prog Nat Sci.,* 2008, **18**, 939-944.